Research article

Zemeng Lin, Xiaowei Li*, Ruizhe Zhao, Xu Song, Yongtian Wang and Lingling Huang*

High-efficiency Bessel beam array generation by Huygens metasurfaces

https://doi.org/10.1515/nanoph-2019-0085
Received March 18, 2019; revised April 20, 2019; accepted April 23, 2019

Abstract: Bessel beams have attracted considerable interest because of their unique non-diffractive, self-healing characteristics. Different approaches have been proposed to generate Bessel beams, such as using axicons, diffractive optical elements, composite holograms, or spatial light modulators. However, these approaches have suffered from limited numerical aperture, low efficiency, polarization-dependent properties, etc. Here, by utilizing dielectric Huygens metasurfaces as ultrathin, compact platforms by integrating the functionalities of Dammann gratings and axicons, we successfully demonstrate multiple Bessel beam generation with polarization-independent property. The number of two-dimensional arrays can be controlled flexibly, which can enhance information capacity with a total efficiency that can reach 66.36%. This method can have various applications, such as parallel laser fabrication, efficient optical tweezers, and optical communication.

Keywords: Huygens metasurfaces; Bessel beams; Dammann gratings.

1 Introduction

Metasurfaces, two-dimensional (2D) counterparts of metamaterials, are designed to modify the characteristics of electromagnetic waves, such as wavefront, intensity distribution, and polarization properties [1–5]. Metasurfaces are usually composed of subwavelength nanoantenna or dielectric resonator (meta-atoms) arrays. Light interaction with metasurfaces is mainly determined by the geometric design as well as material properties. Hence, various building blocks of metasurfaces are proposed to manipulate the electromagnetic properties of scattered fields. To control a wavefront, amplitude modulation and phase control are of paramount importance [6–14]. Huygens metasurfaces (HMSs) are a type of metasurface used to achieve high-efficiency and flexible phase manipulation [15, 16]. For simplicity, based on Huygens' principle, HMSs can function as a combination of orthogonal electric and magnetic dipoles; therefore, the secondary sources reradiate the incident field into the far field through scattering with near-unity efficiency [17]. In particular, by utilizing an HMS composed of a cylinder nanopost array, polarization-independent characteristic can also be achieved for isotropic building blocks.

Bessel beams exhibit a collimated non-diffraction characteristic and possess the form of a Bessel function of the first kind. This beam was discovered when Durnin solved Whitaker's solutions of the Helmholtz equation in 1987 [18]. Because of their unprecedented characteristics, Bessel beams have various applications in optical alignment, interconnection, molecular detection, microscopic imaging, and other areas [19, 20]. Traditionally, Bessel beams are generated using axicons, diffractive optical elements, composite holograms, or spatial light modulators [21–23]. The use of axicons is limited for low-numerical-aperture (low-NA) and wavelength-dependent full width at half maximum (FWHM) ($\mathrm{FWHM}_{J_0} = \frac{0.358\lambda}{\mathrm{NA}}$, for zero-order Bessel beam). These challenges can be overcome with an optical system composed of annular apertures and a high-NA lens, while the transmission efficiency is limited because a considerable amount of light energy is blocked by annular apertures. Compared with single-Bessel-beam generation, multiple-Bessel-beam array generation has the advantages of parallel processing and large capacity, which can be applied in parallel laser fabrication, time-saving atomic transport and cell transfection, multiple imaging, and coherent summation of laser beams [24–26]. However, traditional multiple-Bessel-beam array generation uses the spatial light modulator

***Corresponding authors: Xiaowei Li,** Laser Micro/Nano-Fabrication Laboratory, School of Mechanical Engineering, Beijing Institute of Technology, Beijing 100081, China, e-mail: lixiaowei@bit.edu.cn; and **Lingling Huang,** School of Optics and Photonics, Beijing Institute of Technology, Beijing 100081, China, e-mail: huanglingling@bit.edu.cn. https://orcid.org/0000-0002-3647-2128
Zemeng Lin, Ruizhe Zhao, Xu Song and Yongtian Wang: School of Optics and Photonics, Beijing Institute of Technology, Beijing 100081, China

tool to divide it into many subdomains to provide multiple axicon phase-masks. This method is inefficient and suffers from inhomogeneity of energy distribution and interference-induced oscillations, which result in very low quality. Note the fact that a subdomain structure cannot reach high NA as compared with the proposed metasurface design in the same size.

In previous works, both in-plane surface wave and out-of-plane free wave modulation have been demonstrated for Bessel beam generation with metasurfaces. In the near-field region, by utilizing intersecting metallic gratings or quasi-phase-matching conditions, collimated SPP (surface plasmon polariton) waves possessing Bessel properties can be generated [27, 28]. Using a holographic principle, a surface wave functioning as a reference beam can interfere with the holographic pattern of metasurfaces, which can reproduce interfering leaky waves forming a Bessel beam in near fields [29]. This in-plane Bessel beam generation has the disadvantage that energy vanishes in a short length. For out-of-plane propagation, by utilizing titanium dioxide (TiO_2) nanoposts, Wei et al. generated a single Bessel beam with a focal length of 75 μm for the incident wavelength of 405 nm [30]. Another work employed gradient cascaded metasurfaces to bend terahertz beams in anomalous refraction directions and to generate a non-diffractive Bessel beam under normal and oblique incident conditions [31]. However, such a cascaded metasurface is still very difficult to achieve in the optical regime. The abovementioned methods focused on the generation of a single Bessel beam. These demonstrations with metasurfaces are still lacking for multiple-Bessel-beam array generation.

In this study, a dielectric HMS was used to generate multiple Bessel beams with high efficiency and an ultracompact footprint. The HMS is composed of cylinder nanoposts with a tailored radius and possesses polarization-independent properties. By combining the Dammann grating concept with the Bessel function, we achieved the axicon-like phase-mask for 5×5, 2D Bessel beam generation. The non-diffraction propagation lengths were characterized, and the measured experimental efficiency could reach as much as 66.36%. Meanwhile, the FWHM of the generated Bessel beam is about 1600 nm. The theoretical investigations and experimental demonstrations agree well with each other. Our proposed method can also be extended to generate higher-order Bessel vortex beams by adding a spiral phase to the existing phase-mask. Therefore, multiple Bessel beam generations based on metasurfaces can significantly benefit applications in scanning microscopy, optical manipulation, and lithography to achieve a high spatial resolution and parallel processing.

2 Design principles and results

As shown in Figure 1A, by illuminating arbitrary polarized light on the designed dielectric HMS, 5×5 Bessel beam arrays are generated with high uniformity. The scalar form of a Bessel beam propagating along the z-axis in the cylindrical coordinates (r, φ, z) can be expressed as $E(r, \phi, z) = A \exp(ik_z z) J_n(k_r r) \exp(\pm in\phi)$, where A is the amplitude, J_n is an nth-order Bessel function, k_z and k_r are the corresponding longitudinal and radial wavevector, respectively, and obey the relation $\sqrt{k_z^2 + k_r^2} = k = \frac{2\pi}{\lambda}$, where λ is the wavelength. For the zero-order ideal Bessel beam, its intensity has the maximum value in the center, and the side lobes decay fast away from the main lobe in the plane orthogonal to the propagation direction, as shown in Figure 1B and C. Furthermore, the radial intensity is independent of the z-direction. Note that an ideal Bessel beam solution carries infinite energy, because it is not square integrable; therefore, it cannot be realized in practice. Nevertheless, it is possible to experimentally approach the ideal Bessel solution by modulating it with a Gaussian envelope, axicon envelope, etc. Thus, a quasi-Bessel beam can be experimentally generated, and it has limited focal depth over a distance.

For multiple-Bessel-beam generation, an HMS was designed by combining the Dammann grating concept with the axicon phase profile. Usually, a Dammann grating

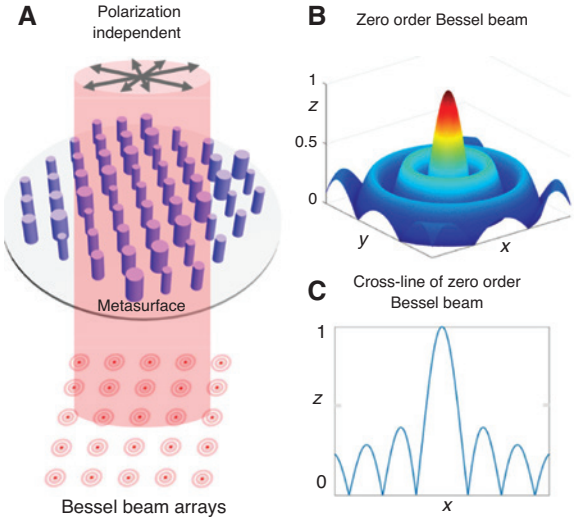

Figure 1: Schematic of the Bessel beam array generation based on HMS.
The gray arrows indicate the polarization of the incident light: (A) illustration of HMS composed of nanoposts to generate Bessel beam arrays; (B) 3D image of a Bessel beam; and (C) the cross-section line of a single Bessel beam.

is a pure phase modulation grating whose phase transition points are optimized to produce equal-intensity spots at diffractive orders with high efficiency. To ease the nanofabrication while avoiding ultra-small transition points, multi-order phase optimization by using periodic lattices of the metasurface was chosen. The design principle for the Dammann grating is as follows. For a 2D multiorder phase grating, its complex transmission can be expressed as $t(x, y) = \exp[i\theta(x, y)]$, which represents the spatial distribution of complex amplitude. Without loss of generality, the Dammann grating is composed of periodic arranged supercells, and each supercell is divided into 10×10 units with various phase distributions. Here, the unit size (equal to the pixel size of the metasurface) is chosen to be 400 nm, and the period of supercell d_0 is 4 μm. The phase of each unit cell can be optimized with a simulated annealing method or genetic algorithm to achieve the 5×5 diffraction orders with equal intensities while suppressing all the other unwanted orders. By setting optimal targets and several iterations, we can obtain the optimized phase distribution of such supercell composed of 10×10 units, as shown in the inset of Figure 2A. The fractional phase profile of the optimized Dammann grating phase distribution is shown in Figure 2A for visualization, whereas the total size of the whole distribution is 800×800 pixels (80×80 supercells). The axicon phase is shown in Figure 2B. Note that the NA of the metasurfaces is defined as $\frac{\sqrt{m^2 + n^2}\lambda}{d}$, where (m, n) is the grating order in x and y directions, and d is the period of the supercell. Then, the calculated NA is 0.55.

Meanwhile, the classical axicon profile is given by $g(r) = \exp[i\varphi(r)] = \exp(-i2\pi r/r_0)$, where $r = \sqrt{x^2 + y^2}$ in the radial coordinate and r_0 is an adjustable control parameter that determines the diameter of the Bessel beam. The phase function $\varphi(r) = 2\pi r/r_0$ creates a beam with an approximate Bessel function profile that remains constant over a distance $z_{max} = Dr_0/2\lambda$, where D is the diameter of the phase-mask. Considering the Nyquist sampling limit $r_0 = p\Delta$ in theoretical calculations, this means the original signal can be restored after transmission with a sampling rate $p_{min} = 2$, and Δ is the lattice constant. Here, we set $p = 100$.

Hence, the key for quasi-Bessel beam array generation is integrating the axicon function with the Dammann grating. The final generated phase pattern can be written as $g(r, \theta) = \exp(-i2\pi r/r_0)\exp(i2\pi x/d_0)$, where d_0 is the supercell period of the Dammann grating, as shown in Figure 2C. We carefully choose the pixel size and grating period to ensure that all the 5×5 diffraction orders can be sufficiently collected by the objective. The relative size of the Bessel beam

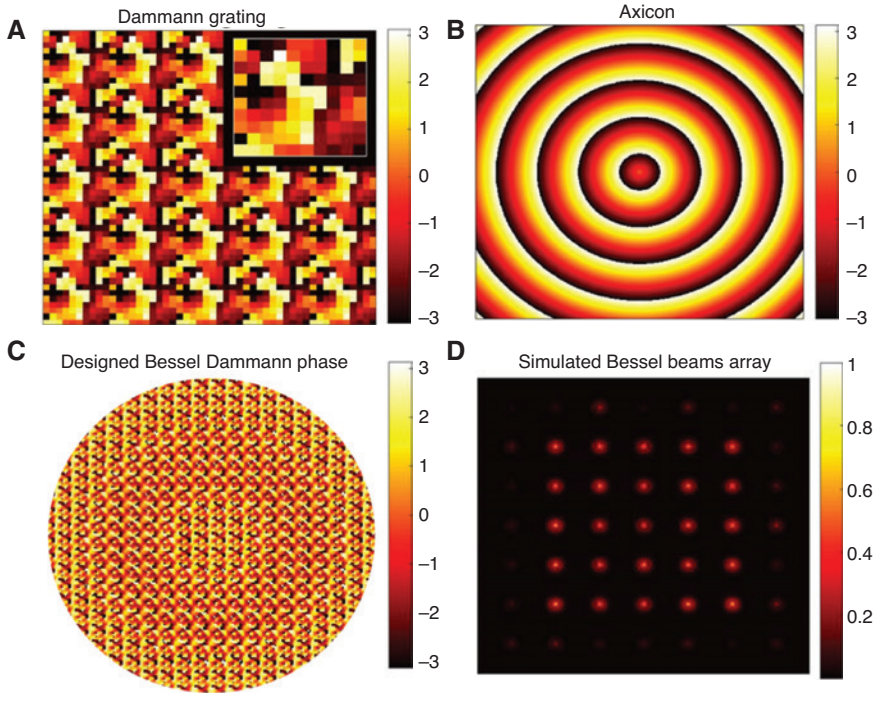

Figure 2: Simulation results of Bessel beam array.
The following is the design process of the metasurfaces and Bessel beam generation: (A) fractional phase profile of the Dammann grating (the inset is the optimized phase distribution within one supercell); (B) phase profile of axicon; (C) final Bessel phase profile by integrating Dammann grating with axicon function; and (D) numerical reconstruction of Bessel beams by using Fresnel propagation.

can be adjusted by the number and size of supercells. According to the Fresnel diffraction function, we have $U(x,y)=\frac{\exp(jkd)}{j\lambda d}\int_{-\infty}^{\infty}\int_{-\infty}^{\infty}U_0(x_0,y_0)\exp\left\{\frac{jk}{2d}[(x-x_0)^2+(y-y_0)^2]\right\}dx_0dy_0$, where $U(x,y)$ and $U_0(x_0,y_0)$ represent the complex amplitude of the image plane and object plane, respectively, and $k=\frac{2\pi}{\lambda}$ is the wavevector, while d is the propagation length. Using the function, we can simulate the propagation of the generated Bessel beam; therefore, we obtain the 5×5 Bessel beam array in the Fresnel zone with a reconstruction distance of 4 mm, as shown in Figure 2D.

The dielectric HMSs are composed of a nanopost array on top of a glass substrate, as shown in Figure 3A. To achieve the desired phase distributions, a 2D parameter optimization was performed using the finite-difference time domain method. Because the absorption in the optical regime is relatively low and much easier to fabricate, we chose silicon nanoposts as building blocks. We start with the wavelength and height sweep, as shown in Figure 3C and D. The height ranges from 200 to 600 nm with a period of 400 nm, while the wavelength λ covers 550–1000 nm. At a fixed wavelength of 780 nm, the height of the cylinder is not an important index to induce the desired phase change. For the convenience of fabrication and experiment, we choose height $h=450$ nm and $\lambda=780$ nm for further optimization. The corresponding refractive index of the silicon cylinder in the simulation is $n_{si}=3.8502+0.01092*1i$, and, for the substrate, it is $n_{SiO_2}=1.5$. The refractive index of Si can match the experimentally measured value with ellipsometry, which is $n_{ell}=3.62015+0.00164*1i$. A 1D sweep was conducted by varying the radius in the range from 40 to 115 nm, with a period of 400 nm. Figure 3B shows that the radius of the nanopost is a dominant parameter to induce a drastic phase shift for the transmission light. The amplitude of the output light is relatively uniform and has >60% efficiency. Note that the transmission efficiency of the metasurface is determined by the intrinsic material loss (the absorption) and also by the geometric design (related to scattering or reflection). Meanwhile, the phase can cover $0–2\pi$, which enables the full modulation property. Eight-order phase levels were obtained that cover the range of 2π to map the theoretical phase distribution. Then, the total phase-mask distribution is encoded into the HMSs.

The metasurface sample was fabricated following the processes of deposition, patterning, lift off, and etching.

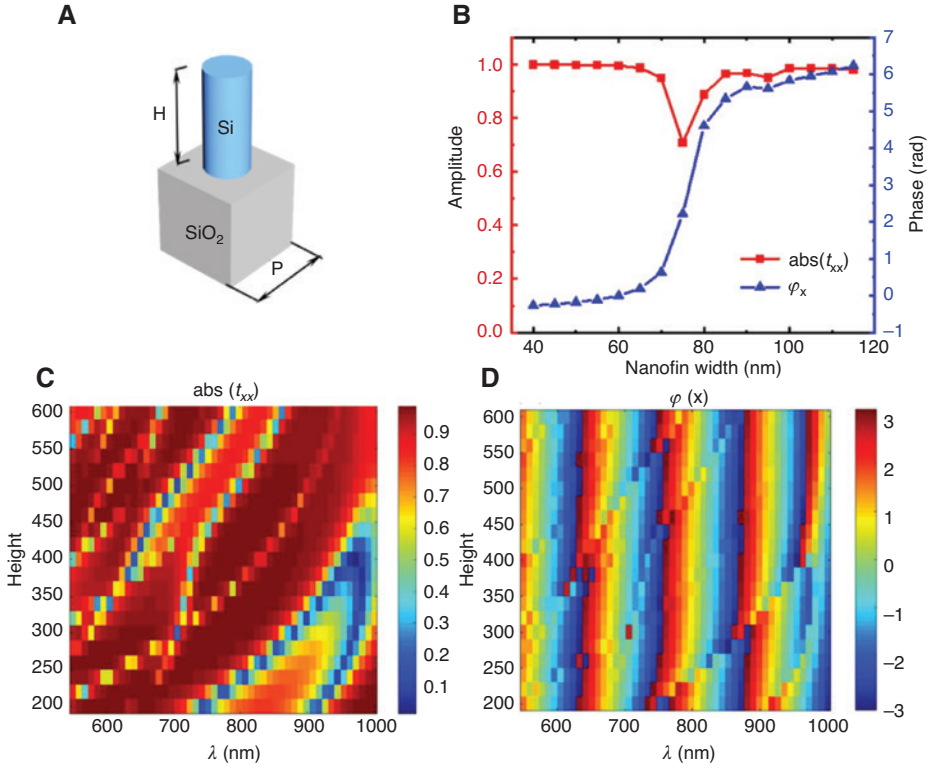

Figure 3: Simulation of the HMS.
(A) The unit cell composed of cylinder nanopost above the silica substrate. (B) Parameter sweep of amplitude and phase by varying the radius of nanopost. (C, D) 2D sweep by varying the incident wavelength and height of nanopost.

The top- and side-view scanning electron microscopy (SEM) images are shown in Figure 4A and B. The geometric parameters of the nanoposts correspond to the theoretical designs. The experimental setup for the far-field characterizing and imaging is shown in Figure 4C. The laser beam with a wavelength of 780 nm passed through a polarizer and impinged on the sample. After interacting with the sample, the transmitted light was collected by an objective with NA = 0.85, 60×, and a lens. To fully harvest the light passing through the sample, the objective was tightly placed after the sample. The generated Bessel beams were recorded using a charge-coupled device (CCD) camera. To obtain the *yz*-plane, the positions of sample, objective, and other components were unchanged, while only the position of the CCD camera was changed using a 3D precision translation stage. Thus, we measured the different propagating distances of the Bessel beam array by referring to the origin point ($z = 0$) of the metasurface.

The experimental results are shown in Figure 5. In the experiment, we detected different *xy*-planes of the Bessel beam in the distance range from 11.25 to 24 mm (the central distance is 17.625 mm) with a step of 0.05 mm; hence, we could record 256 *xy*-planes. Then, post-processing was performed to obtain the desired *yz*-plane. For every *xy*-plane, we can choose either of the five column cross-lines for *yz*-plane propagation. The 5×5 Bessel beam arrays were obtained in the *xy*-plane, as shown in Figure 5A. All the diffraction beams have an almost uniform intensity distribution, while the zeroth order has a relatively large intensity, because of the unavoidable discrete property of the metasurface (light passing through the bare substrate without interaction of nanoposts) and fabrication errors, combined with the misalignment issues, which may result in a large spot size of the zero order compared to a single point. Because the zero-order Bessel beam intensity is too strong, which may affect the surrounding order for visualization, the +1 order 5×1 Bessel beam (white arrow in Figure 5A) was chosen to observe the non-diffraction property in the *yz*-plane, as shown in Figure 5B. Such Bessel beams possess a tightly focused waist and have ignorable divergence in propagation direction. To demonstrate Bessel beam generations more clearly, we compared the cross section of a single beam in the experiment (Figure 5C) with the one in the simulation (Figure 5D). The beam width is dependent on both the auxiliary objectives/lens and the design of the metasurface itself. Both cross sections show a quasi-Bessel-like profile; hence, the experimental results are consistent with the simulations. Because of the limited spatial resolution of the CCD, the side lobes are not as perfect as the ideal cases.

Meanwhile, the captured Bessel beam intensities at different orders were not strictly identical in the experimental results because of alignment-related problems. The angle of each diffraction order can be easily determined by using grating equations. In our experiment, the maximum diffraction angle was 22.9°; therefore, we could ensure that all the diffraction orders could be collected using the objective. By replacing the CCD camera with a power meter, we measured the efficiency of all the diffraction orders. The diffraction efficiency is defined as the ratio of the power of the output light of all the diffraction orders (excluding the zero-order energy) to the power of the incident light. A dielectric HMS can provide a much higher efficiency than traditional methods, with an efficiency of as much as 66.36%. Furthermore, by optimizing the phase distribution of the Dammann grating, we can easily achieve an arbitrary 2D beam array.

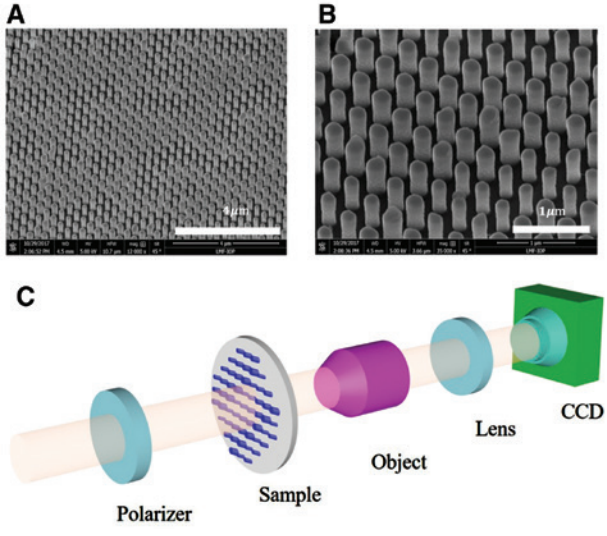

Figure 4: Sample fabrication and experimental setup. (A, B) Side view of the SEM images of the HMS. (C) Experimental setup for the characterization of metasurface.

3 Conclusion

In summary, we proposed and demonstrated a dielectric HMS composed of cylinder nanoposts for 2D 5×5 Bessel beam array generation by integrating the Dammann grating concept with an axicon phase-mask. The phase modulation was based on the electric and magnetic resonance effect within the high-index Si nanoposts to mimic a Huygens source. HMS can provide phase modulation capability covering the 2π range, while maintaining

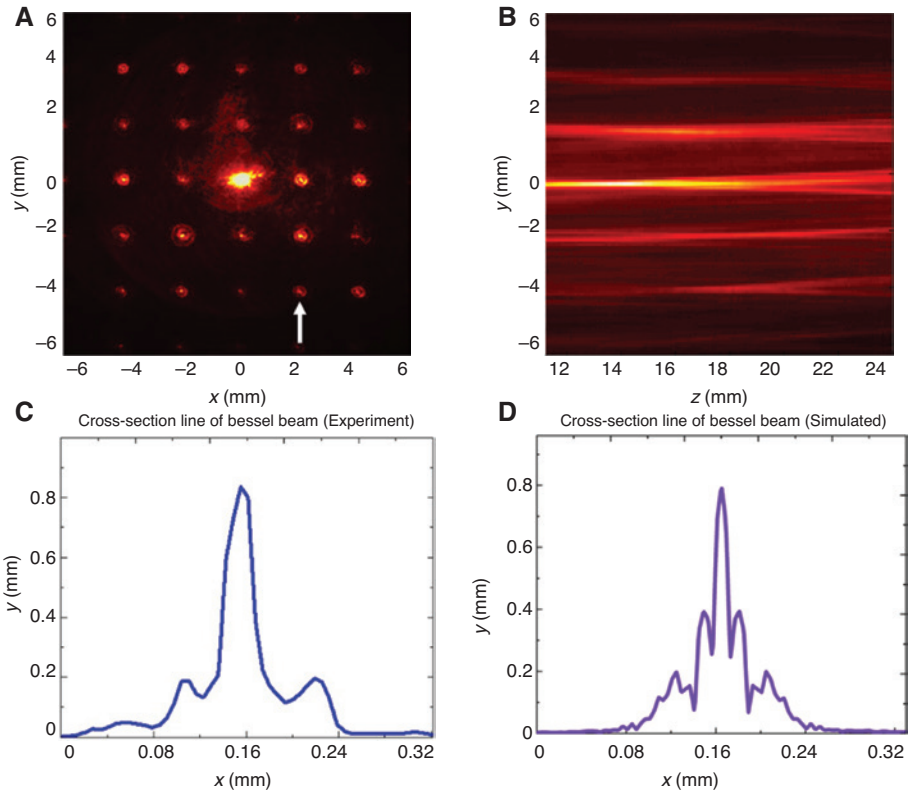

Figure 5: Experimental results of the Bessel array generation.
(A) Experimental results of the generated 5 × 5 Bessel beam arrays in *xy*-plane (the white arrow indicates the orders used to retrieve the *yz*-plane). (B) Non-diffraction propagation property of the Bessel beam arrays in *yz*-plane (the five main orders of the Bessel beams can be clearly observed). (C) Line cross-section corresponding to one of the Bessel beams in *xy*-plane. (D) Line cross-section corresponding to one of the Bessel beams in *xy*-plane.

uniform amplitude. Optical characteristic measurements were carried out to determine the long-range non-diffraction properties. HMS has the advantages of compactness, high efficiency, and relatively easy fabrication properties. The generated Bessel beam array has great potential in various applications, with benefits for parallel laser fabrication, molecule transportation, cell detection, optical communications, and other fields.

Acknowledgments: The authors acknowledge the support from the National Natural Science Foundation of China (Funder Id: http://dx.doi.org/10.13039/501100001809, no. 61775019, 51675049) program, the Beijing Municipal Natural Science Foundation (Funder Id: http://dx.doi.org/10.13039/501100005089, no. 4172057, 3172027), the Beijing Nova Program (Funder Id: http://dx.doi.org/10.13039/501100005090, no. Z171100001117047), and the Fok Ying-Tong Education Foundation of China (no. 161009).

Conflicts of interest: The authors declare that they have no conflicts of interest.

References

[1] Arbabi A, Arbabi E, Yu H, Kamali SM, Faraon A. Planar metasurface retroreflector. Nat Photon 2017;11:415–20.
[2] Chen HT, Taylor AJ, Yu N. A review of metasurfaces: physics and applications. Rep Prog Phys Soc 2016;79:076401.
[3] Devlin RC, Khorasaninejad M, Chen WT, Oh J, Capasso F. Broadband high-efficiency dielectric metasurfaces for the visible spectrum. Proc Natl Acad Sci USA 2016;113:10473–8.
[4] Genevet P, Capasso F, Aieta F, Khorasaninejad M, Devlin R. Recent advances in planar optics: from plasmonic to dielectric metasurfaces. Optica 2017;4:139–52.
[5] Kuznetsov AI, Miroshnichenko AE, Brongersma ML, Kivshar YS, Luk'Yanchuk B. Optically resonant dielectric nanostructures. Science 2016;354. pii: aag2472-1.
[6] Almeida E, Bitton O, Prior Y. Nonlinear metamaterials for holography. Nat Commun 2016;7:12533.
[7] Amir A, Yu H, Mahmood B, Andrei F. Dielectric metasurfaces for complete control of phase and polarization with subwavelength spatial resolution and high transmission. Nat Nanotechnol 2015;10:937–43.
[8] Deng Z, Deng J, Zhuang X, et al. Diatomic metasurface for vectorial holography. Nano Lett 2018;18:2885–92.
[9] Han N, Huang L, Wang Y. Illusion and cloaking using dielectric conformal metasurfaces. Opt Express 2018;26:31625–35.

[10] Jierong C, Davood AOB, Hossein M. Wave manipulation with designer dielectric metasurfaces. Opt Lett 2014;39:6285–8.
[11] Wei Q, Huang L, Li X, Liu J, Wang Y. Broadband multiplane holography based on plasmonic metasurface. Adv Opt Mater 2017;5:1700434.
[12] Ye W, Zeuner F, Li X, et al. Spin and wavelength multiplexed nonlinear metasurface holography. Nat Commun 2016;7:11930.
[13] Zhao R, Sain B, Wei Q, et al. Multichannel vectorial holographic display and encryption. Light Sci Appl 2018;7:95.
[14] Zheng G, Mühlenbernd H, Kenney M, Li G, Zentgraf T, Zhang S. Metasurface holograms reaching 80% efficiency. Nat Nanotechnol 2015;10:308–12.
[15] Decker M, Staude I, Falkner M, et al. High-efficiency light-wave control with all-dielectric optical Huygens' metasurfaces. Adv Opt Mater 2015;3:813–20.
[16] Kim M, Wong AMH, Eleftheriades GV. Optical Huygens' metasurfaces with independent control of the magnitude and phase of the local reflection coefficients. Phys Rev X 2014;4:181.
[17] Chen M, Kim M, Wong AMH, Eleftheriades GV. Huygens' metasurfaces from microwaves to optics: a review. Nanophotonics 2018;7:1207–31.
[18] Durnin J. Exact solutions for nondiffracting beams. I. The scalar theory. J Opt Soc Am A 1987;4:651–4.
[19] Ahluwalia BPS, Yuan XC, Tao SH, et al. Microfabricated-composite-hologram-enabled multiple channel longitudinal optical guiding of microparticles in nondiffracting core of a Bessel beam array. Appl Phys Lett 2005;87:084104.
[20] Wang Z, Jiang L, Li X, et al. High-throughput microchannel fabrication in fused silica by temporally shaped femtosecond laser Bessel-beam-assisted chemical etching. Opt Lett 2017;43:98–101.
[21] Bowman R, Muller N, Zambrana-Puyalto X, Jedrkiewicz O, Trapani PD, Padgett MJ. Efficient generation of Bessel beam arrays by means of an SLM. Eur Phys J Spec Top 2011;199:159–66.
[22] Chu X, Sun Q, Wang J, Lü P, Xie W, Xu X. Generating a Bessel-Gaussian beam for the application in optical engineering. Sci Rep 2015;5:18665.
[23] Liang C, Zhu X, Mi C, et al. High-quality partially coherent Bessel beam array generation: erratum. Opt Lett 2018;43:4939–40.
[24] Cizmár T, Kollárová V, Tsampoula X, et al. Generation of multiple Bessel beams for a biophotonics workstation. Opt Express 2008;16:14024–35.
[25] García-Martínez P, Sánchez-López MM, Davis JA, Cottrell DM, Sand D, Moreno I. Generation of Bessel beam arrays through Dammann gratings. Appl Opt 2012;51:1375–81.
[26] Pfeiffer C, Grbic A. Controlling vector Bessel beams with metasurface. Phys Rev Appl 2014;2:044012.
[27] Jiao L, Jean D, Patrice G, Benoit C, Frederique DF, Federico C. Cosine-gauss plasmon beam: a localized long-range nondiffracting surface wave. Phys Rev Lett 2012;109:093904.
[28] Li L, Li T, Wang SM, Zhu SN. Collimated plasmon beam: nondiffracting versus linearly focused. Phys Rev Lett 2013;110:046807.
[29] Ben Geng C, Bo LY, Xiang JW, Qiang C, Tie Jun C. Generation of spatial Bessel beams using holographic metasurface. Opt Express 2015;23:7593–601.
[30] Wei TC, Khorasaninejad M, Zhu AY, et al. Generation of wavelength-independent subwavelength Bessel beams using metasurfaces. Light Sci Appl 2016;6:e16259.
[31] Liu S, Noor A, Liang LD, Lei Z, Tie Jun C. Anomalous refraction and nondiffractive Bessel-beam generation of terahertz waves through transmission-type coding metasurfaces. ACS Photon 2016;3:1968–77.